ECS Journal of Solid State
Science and Technology

The Electrochemical Society
Advancing solid state & electrochemical science & technology

Laser-Activated Luminescence of BaAl$_2$O$_4$:Eu

View the article online for updates and enhancements.

Laser-Activated Luminescence of BaAl$_2$O$_4$:Eu

Daniel den Engelsen, George R. Fern, Terry G. Ireland,[z] and Jack Silver

Centre for Phosphor and Display Materials, Wolfson Centre for Materials Processing, Brunel University London, Uxbridge, Middlesex, UB8 3PH, United Kingdom

In this article the laser-activated (LA) luminescence of BaAl$_2$O$_4$ doped with 3 mol% Eu^{2+} and SrAl$_2$O$_4$ doped with 700 ppm Eu^{2+} is described. The LA spectrum of BaAl$_2$O$_4$:Eu did not show any emission from Eu^{2+}, but rather luminescence from the Eu^{3+} ion. This surprising result is explained in terms of ionization of the excited Eu^{2+} ions (photo-ionization), while the freed electrons are trapped in an excited state of the F-centre: this is considered to be a deep trap. The temperature of the ferroelectric-paraelectric phase transition in BaAl$_2$O$_4$ has been determined at $\approx$180 °C from the Raman spectra recorded at various temperatures.

Recently we published the crystal structures and photoluminescence (PL) spectra of Sr$_{1-x}$Ca$_x$Al$_2$O$_4$, Ba$_{1-x}$Ca$_x$Al$_2$O$_4$ and Ba$_{1-x}$Sr$_x$Al$_2$O$_4$ doped with Eu^{2+}.[1–3] These studies were followed with an analysis of the cathodoluminescence (CL) spectra of undoped BaAl$_2$O$_4$ and BaAl$_2$O$_4$:Eu^{2+}.[4] In the case of BaAl$_2$O$_4$:Eu^{2+} it was found that by exchanging a small quantity of Ba for Sr, the hexagonal P6$_3$ (ferroelectric) structure changed to the more symmetric hexagonal P6$_3$22 (paraelectric) structure at room temperature.[2] This conclusion was based on the analyses of the PL spectra of Ba$_{1-x}$Sr$_x$Al$_2$O$_4$:Eu^{2+} at x<0.3: this was a confirmation by spectroscopy of the work of Kawaguchi et al.,[5] who discovered this phase transition in Ba$_{1-x}$Sr$_x$Al$_2$O$_4$ without Ln^{2+} dopant using X-ray diffraction (XRD). The ferroelectric-paraelectric transition in pure, undoped BaAl$_2$O$_4$ was described earlier by other workers[6–9] based on X-ray diffraction (XRD), electron diffraction studies and analysis of the infrared (IR) spectrum. From these studies it was concluded that the ferroelectric-paraelectric phase transition in BaAl$_2$O$_4$ takes place between 400 and 450 K, which is substantially higher than room temperature. In view of the extended investigations on the afterglow behaviour of BaAl$_2$O$_4$:Eu^{2+} co-doped with Dy^{3+}, it is surprising that no study has been published that confirmed this phase transition based on spectroscopic properties.[10]

As a natural follow up from our previous work[1–4] on the alkaline earth aluminates doped with Eu^{2+} we decided to investigate undoped BaAl$_2$O$_4$ and BaAl$_2$O$_4$:Eu^{2+} between 298 K and 573 K by laser-activated (LA) spectroscopy. The objective was to obtain spectroscopic evidence of the P6$_3$ → P6$_3$22 phase transformation in BaAl$_2$O$_4$. In the LA spectra of BaAl$_2$O$_4$:Eu^{2+}, which were recorded with a YAG:Nd laser (532.1 nm), we detected only Eu^{3+} transitions with an abnormal temperature behaviour, i.e. increasing spectral radiance upon raising the temperature. This prompted us to propose a new model for the excitation process by the laser beam. The results are reported and discussed in the following sections of this paper. We also measured the LA-spectrum of SrAl$_2$O$_4$:Eu^{2+} at room temperature for comparison with BaAl$_2$O$_4$:Eu^{2+} and literature data.

Experimental

Synthesis.—Table I presents the samples that were investigated in the current study.

Starting materials were: barium carbonate (Alfa Aesar, UK, 99%), strontium carbonate (Sigma Aldrich, UK, 99.9%), aluminum oxide (SASOL Inc., USA), europium oxide (Ampere Industrie, France, 99.99%), and concentrated hydrochloric acid (Sigma Aldrich, UK, 37%). All materials were used as supplied without further purification. BA2 (Ba$_{0.97}$Eu$_{0.03}$Al$_2$O$_4$) was prepared by calcining mixtures of an

appropriate molar ratio of BaCO$_3$, γ-Al$_2$O$_3$ and EuCl$_3$ powders in a flow of 90% N$_2$–10% H$_2$. After calcination the powder was ground by ball milling (Al$_2$O$_3$) for 3 h. The final annealing was at 1350 °C under H$_2$/N$_2$ for 2 h. Sample SA1 (SrAl$_2$O$_4$ doped with 700 ppm Eu) was made using the same procedures. Sample BA1, BaAl$_2$O$_4$ without a detectable Eu concentration, was obtained from ABCR (Karlsruhe, Germany). By X-ray diffraction (XRD) it was determined that ABCR's material had partly been decomposed into BaCO$_3$ and Al$_2$O$_3$ due to prolonged shelf life in air. Before recording the spectra, this material was annealed for 60 h at 950 °C in air; after this treatment it was determined by XRD that the material had the hexagonal P6$_3$ structure of BaAl$_2$O$_4$ ($\sim$100%).

Characterisation and spectroscopy.—The crystallinity of the samples BA1, SA1 and BA2 was verified by X-ray powder diffraction using a Bruker D8 Advance X-ray diffractometer fitted with a nickel-filtered copper source, CuKα at λ=1.5406 Å, and a LynxEye™ silicon strip detector.[10] BA1 and BA2 had the hexagonal P6$_3$ phase,[11] whereas SA1 had the monoclinic P2$_1$ phase.[12]

Laser-induced fluorescence spectra of the samples were measured with a Horiba Jobin Yvon Labram HR monochromator by excitation with a Nd:YAG laser (second harmonics at 532.1 nm) at temperatures varying between 25 °C and +300 °C in steps of 25 °C or sometimes 50 °C. Upon stepping from one temperature to another the effects of temperature drift had to be nullified. This was done by monitoring the position of the laser spot on the sample by a microscope and careful manual readjustment using the automated microscope stage of prominent surface features as a marker. The temperature of the sample during measurements was controlled using a TMS600 heating and cooling stage, which used a TMS94 temperature controller with a temperature accuracy of +/−0.1 °C. The morphology of the samples was investigated in a transmission electron microscope (TEM), (2100 F, JEOL, Japan) equipped with a Schottky-type field emission gun.
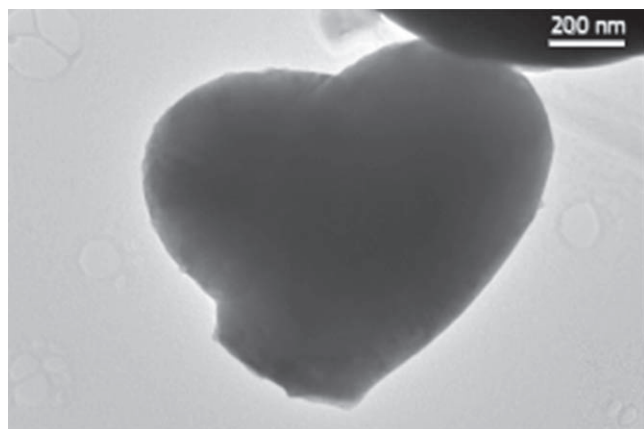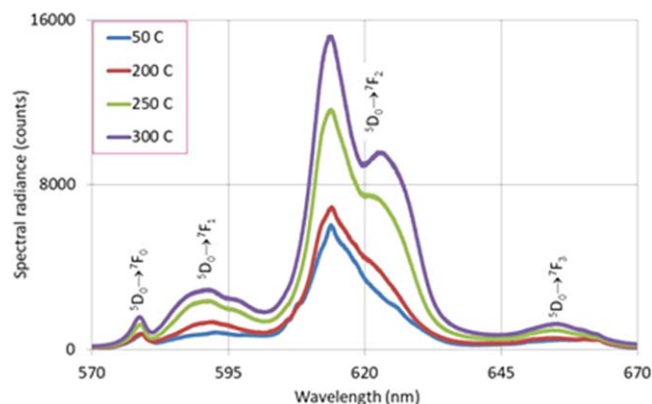
Results

Morphology and structure.—Figure 1 presents a TEM-image of a particle in the BA2 sample. The size of the particles in the samples varied between about 0.5 μm to about 5 μm. From the XRD patterns recorded at room temperature it was concluded that the BaAl$_2$O$_4$ samples listed in Table I consisted of one phase, namely the hexagonal P6$_3$ structure (ferroelectric).[2–4,11]

Laser-activated spectrum.—Fig. 2 presents the Stokes spectra of BA2 between 570 nm and 670 nm recorded at various temperatures. The emission peaks in these spectra can be assigned to BaAl$_2$O$_4$:Eu^{3+}. No Eu^{2+} emission at any temperature between 25 °C and 300 °C was observed in the LA spectra, neither in the anti-Stokes part (λ<532 nm),
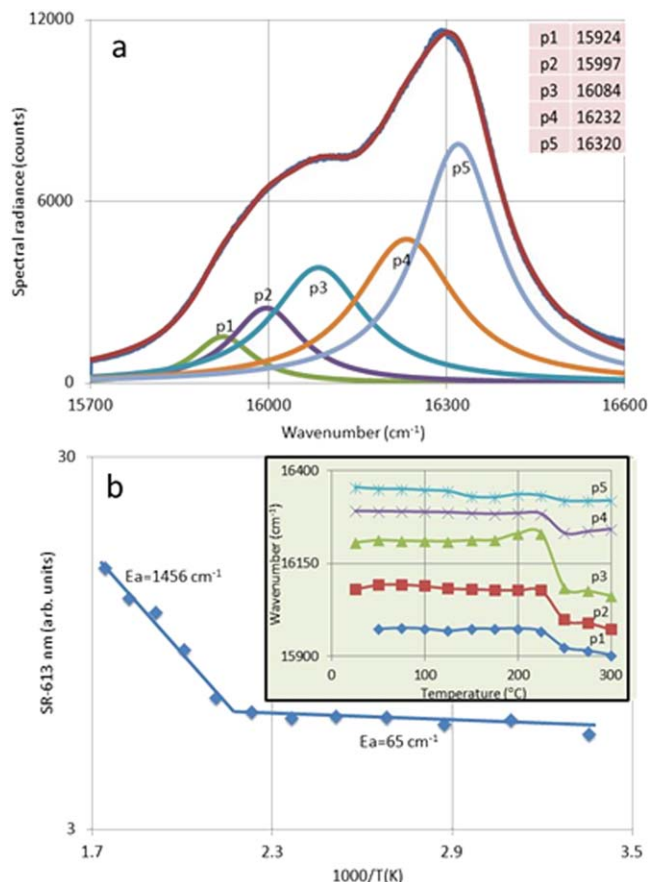
^{z}E-mail: terry.ireland@brunel.ac.uk

Figure 1. TEM images of BaAl$_2$O$_4$:Eu^{2+} (BA2) measured at 200 keV and −169 °C.

Figure 2. LA spectra of BaAl$_2$O$_4$:Eu^{3+} between 570 nm and 670 nm at various temperatures (indicated in °C). The peaks can be assigned to the 4f→4f transitions of Eu^{3+}. For reasons of clarity only a limited number of spectra have been displayed.

Figure 3. (a) Deconvolution of $^5D_0 \rightarrow {}^7F_2$ multiplet of BaAl$_2$O$_4$:Eu^{3+} with 5 Lorentzian profiles. The profiles were fitted to the LA-spectrum with a least squares algorithm using the Excel solver. The LA- spectrum was recorded at 250 °C. The wavenumbers at the maximum spectral radiance (ν_0) of the profiles are indicated in cm^{-1}. (b) Arrhenius plot of the spectral radiance at 613 nm (highest peak of the $^5D_0 \rightarrow {}^7F_2$ multiplet of BaAl$_2$O$_4$:Eu^{3+}. The insert shows ν_0 of the profiles, defined in (a), as a function of the temperature.

nor in the Stokes part. It should be noted that these Eu^{3+} bands were not detected in the PL and Cl spectra in our previous study of this sample,[4] although the Eu^{3+} emission bands in Fig. 2 are rather strong. The spectrum at T = 50 °C in Fig. 2 is similar to the PL spectrum of hexagonal BaAl$_2$O$_4$:Eu^{3+} published by Chatterjee et al.[13] and slightly less similar to the PL spectrum of orthorhombic BaAl$_2$O$_4$:Eu^{3+} measured by Wiglusz and Grzyb.[14] Saturation effects in the LA-spectra of BaAl$_2$O$_4$:Eu^{2+} were separately checked by varying the power density of the laser beam. This was done by inserting 6 different filters in the beam. It was found that the spectral radiances of the 417 cm^{-1} Raman line (in Fig. 4) and the Eu^{3+} $^5D_0 \rightarrow {}^7F_1$ transition at 592 nm vary proportionally with the filter factors between 0.1% and 100%. This result indicates that saturation effects are not expected to play a role. In two recent articles a similar approach about the presence of saturation in the spectra of phosphors has been described,[15, 16]

The absence of any Eu^{2+} luminescence and the presence of rather strong Eu^{3+} luminescence from hexagonal BaAl$_2$O$_4$:Eu cannot be explained by incomplete reduction during the annealing in the H$_2$/N$_2$ flow, because most of the Eu will still be present in the form of Eu^{2+}. In the discussion section a model will be introduced that explains the suppression of any Eu^{2+} emission and the presence of Eu^{3+} lines only. Figure 2 features a rather unusual behaviour of the emission bands, namely a substantial increase of the spectral radiance of all Eu^{3+} transitions at T > 200 °C instead of decreasing luminescence due to thermal quenching. This can clearly be observed in the growth of the shoulder of the $^5D_0 \rightarrow {}^7F_2$ multiplet at 622 nm from 200 °C onwards. This phenomenon will also be explained in the discussion section.

An analysis illustrating the characteristics of the LA-spectra of Fig. 2 is shown in Fig. 3. Fig. 3a presents the result of the deconvolution of the Eu^{3+} $^5D_0 \rightarrow {}^7F_2$ multiplet recorded at 250 °C with 5 lorentzian profiles, while Fig. 3b is an Arrhenius plot of the maximum spectral radiance of the $^5D_0 \rightarrow {}^7F_2$ multiplet (at 613 nm). We decided to evaluate the activation energy from the maximum spectral radiance instead of the radiance, which is the integrated spectral radiance of one profile, because the deconvolution of the $^5D_0 \rightarrow {}^7F_2$ multiplet with 5 strongly overlapping Lorentzian profiles has inaccuracies. Moreover, the temperature dependence of the individual profiles presented some differences. The error made in this way is only ~5%, because the effect of line broadening has been partially included by the summation of the profiles.

The insert of Fig. 3b shows the wavenumbers of the Stark components of the $^5D_0 \rightarrow {}^7F_2$ multiplet as a function of temperature.

The Arrhenius plot in Fig. 3b indicates a change in the temperature behaviour around 185 °C, while the insert shows a
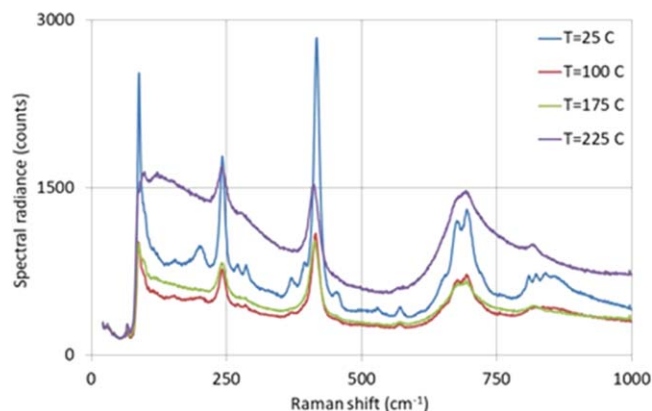
Figure 4. Raman spectra of $BaAl_2O_4$:Eu (BA2) at various temperatures, indicated in °C.

Table II. Lowest 4 f levels of Eu^{3+} in $BaAl_2O_4$ at 25 °C and 300 °C for the $P6_3$ and $P6_322$ phases respectively (in.cm^{-1}).

State	$P6_3$	$P6_322$
$^5D_0$	17262	17281
	1289	1378
	1182	1310
$^7F_2$	1050	1219
	972	1038
	912	961
	568	522
$^7F_1$	385	367
	218	239
$^7F_0$	0	0

kink in the ν_0 curves at about 225 °C. The spectral radiance at 613 nm (SR613) is largely determined by the p5 profile shown in Fig. 3a. We assume that both the change in SR613 and the kinks in the ν_0 curves are related to the transformation of $BaAl_2O_4$ from the ferroelectric $P6_3$ phase to the paraelectric $P6_322$ phase. Because of the change of the crystal structure of $BaAl_2O_4$, the crystal field for the Eu ions modifies, which means that the radiance ratio(s) between the 5 Stark components of the $^5D_0 \rightarrow {}^7F_2$ multiplet changes as well. In Table II we have summarized the Stark levels of the $^5D_0 \rightarrow {}^7F_J$ (J = 1, 2) multiplets at room temperature for the $P6_3$ phase of $BaAl_2O_4$:Eu^{3+} and at 300 °C for the $P6_322$ phase.

The Eu^{3+} $^5D_0 \rightarrow {}^7F_0$ transition at 579 nm was also analysed, as it has only one Stark component. In view of this it would be expected to be symmetric, however this peak is asymmetric at 25 °C and at T > 200 °C and this asymmetry must indicate the presence of at least two overlapping luminescence peaks. Because of the $P6_3 \rightarrow P6_322$ phase transition at about 185 °C, it would be expected that the 579 nm transition has a symmetric profile at T > 200 °C, because the $BaAl_2O_4$ $P6_322$ phase has only one Ba site, and thus would be expected to have only one Eu site. Since this is not the case (as evidenced by the asymmetry, then there are only to our minds two possible explanations), either some sort of electron-phonon coupling is occurring or the Eu^{3+} cations being much smaller than the Ba^{2+} cations find two or more positions in the sites that each give rise to a slightly different $^5D_0 \rightarrow {}^7F_0$ transition hence generating the overall asymmetric band.

Fig. 4 presents the Raman spectra of BaAl2O4:Eu2 + recorded at various temperatures.

For clarity reasons only a limited number of spectra have been displayed in Fig. 4. The spectrum recorded at 25 °C indicates the presence of a rather large number of weak Raman lines, which gradually disappear at high temperature. Table III summarizes the

Table III. Raman-active lines of $BaAl_2O_4$:Eu^{2+} at 25 °C and 225 °C and IR-active transitions (from Rodehorst et al.[9]).

T = 25 °C RS (cm^{-1})	Int.	T = 225 °C RS (cm^{-1})	Int.	Rodehorst et al.[9] Freq. (cm^{-1})	Int.
156	w			140	m
200	w			160	m
242	ms	240	w	230?	vw
270	w				
371	w				
383	w				
417	s	411	s	415	s
457	w				
528	w				
570	w	566	vw		
654	w			620	s
663	m	671	m		
705	m	692	m		
809	w			810	m
821	w	816	w		
850	w			830	m

observed Raman-active transitions in the spectra of Fig. 4. lazic et al.[17] published the Raman spectrum of $Ba_3Al_2O_6$, which adopts the cubic subgroup $P2_13$. As expected, the lattice vibrations differ substantially; however, in the tribarium aluminate a Raman line at 248 cm^{-1} was measured, which is close to the Raman line at 242 cm^{-1} in $BaAl_2O_4$. Lazic et al. assign this line tentatively to a vibration of the ring formed by the AlO_4 tetrahedra.

RS in Table III stands for Raman shift. For comparison reasons, the IR-active transitions of $BaAl_2O_4$, measured by Rodehorst et al.[9] at room temperature, have been included in Table III. Table III indicates that the majority of the weak Raman lines at 25 °C have disappeared at 225 °C. The Raman shift of the Raman-active lines of sample BA1 (with no detectable Eu^{3+}) is generally ~1.5 cm^{-1} higher. For instance the two strong Raman lines for this sample are at 243.6 cm^{-1} and 418.7 cm^{-1} at room temperature.

The Raman lines in Fig. 4 are narrow and can adequately be represented by Lorentzian profiles. This is shown in Fig. 5a for a part of the spectrum recorded at 25 °C. The full width at half maximum (FWHM) of the Raman lines increases substantially when the temperature is increased. In Fig. 5b the radiance (integrated intensity) of the Raman profile p1 (at 200 cm^{-1}) has been plotted versus temperature.

The Raman line at 200 cm^{-1} and the other w-lines listed in the first column of Table III (except the lines at 570 cm^{-1} and 821 cm^{-1}) disappear at about 175 °C. This is shown in Fig. 5b for the 200 cm^{-1} line. Note that the radiance decreases gradually: there does not seem to be an abrupt change at ≈175 °C. In the transition from the hexagonal $P6_3$ structure of $BaAl_2O_4$ to the hexagonal $P6_322$ structure the number of Raman active lines reduces from 82 to 15[9]: indeed, in Fig. 4 and Table III a large reduction of the number of Raman lines upon increasing the temperature beyond 175 °C is observed. So, it can be concluded that Fig 4 and 5 provide additional spectroscopic evidence of the ferroelectric → paraelectric transition in $BaAl_2O_4$. Herein this transition is found at slightly higher temperature than indicated by Huang et al.[6,7] at the same temperature as published by Kawaguchi et al.[5] and Rodehorst et al.[9] and inside the range of temperatures reported by Abakumov et al.[8]

Fig. 6 is the LA-spectrum of SA1 between 570 nm and 630 nm at room temperature. This spectrum also shows the Eu^{3+} $^5D_0 \rightarrow {}^7F_J$ (J = 0, 1, 2) transitions; however, the lines are much narrower at a low Eu concentration than the partially overlapping peaks in Fig. 2. The arrows in Fig. 6 indicate very weak lines, which are tentatively assigned to $^5D_0 \rightarrow {}^7F_J$ (J = 0, 1, 2) transitions of Eu^{3+} ions at the other alkaline earth site in the monoclinic $SrAl_2O_4$ structure. In
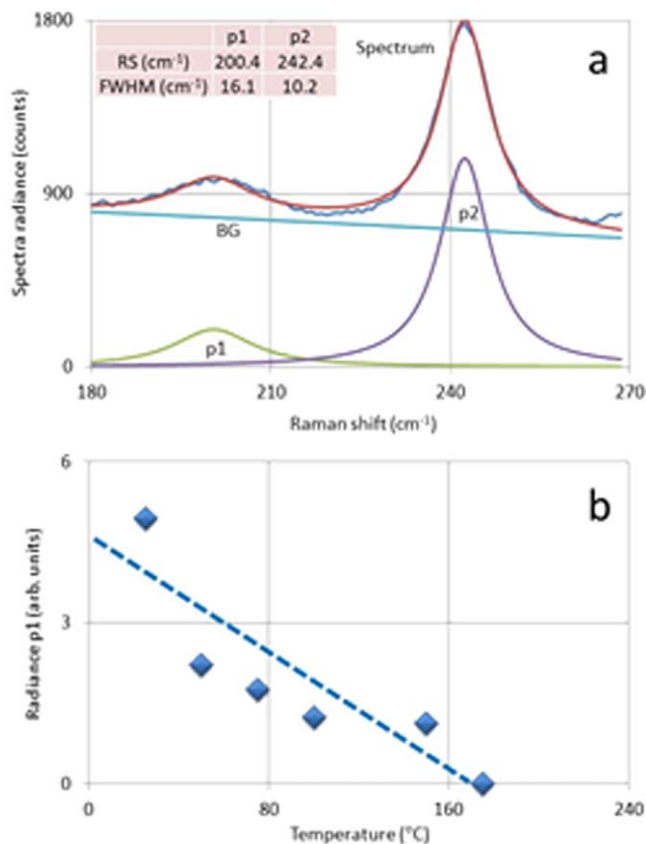
Figure 5. (a) Deconvolution with two Lorentzian profiles of the Raman spectrum of $BaAl_2O_4$:Eu (BA2) recorded at 25 °C. BG is the background level. The insert represents the Raman shifts (RS) at maximum spectral radiance and the FWHMs in cm^{-1} of the two profiles. (b) Radiance of p1 profile (200 cm^{-1}) from (a) versus temperature.
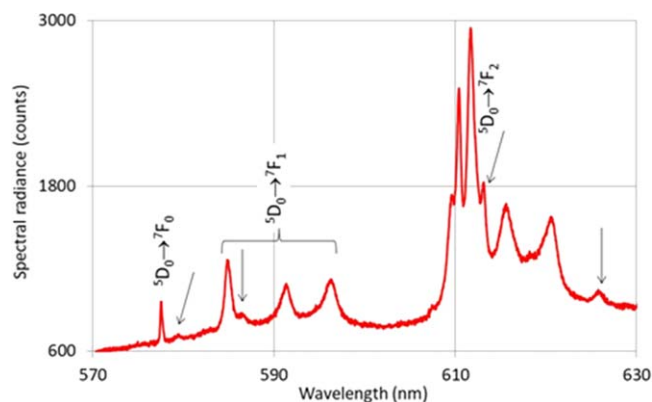

Figure 6. Part of LA-spectrum of $SrAl_2O_4$:Eu^{3+} (SA1) recorded at room temperature. The arrows indicate weak electronic transitions of Eu^{3+} at the other site in the monoclinic crystal.

Fig. 7 the Raman spectra of $BaAl_2O_4$ and $SrAl_2O_4$ have been plotted for comparison reasons.

The Raman spectra $BaAl_2O_4$:Eu (BA2) and $SrAl_2O_4$:Eu (SA1) in Fig. 7 present strong Raman lines at 418 cm^{-1} and 468 cm^{-1} respectively, which could indicate a similar vibrational origin generating these lines. In this energy range internal vibration modes of the AlO_4 tetrahedra are expected.[17] If this is the case, then the coupling with the vibration of the alkaline earth ion cannot be neglected. The three strongest lines in the Raman spectrum of $SrAl_2O_4$ have been indicated in Fig. 7. The Raman spectrum of $SrAl_2O_4$ presented in Fig. 7 agrees with the Raman spectra published by Dong et al.[18] and Terraschke et al.[19]
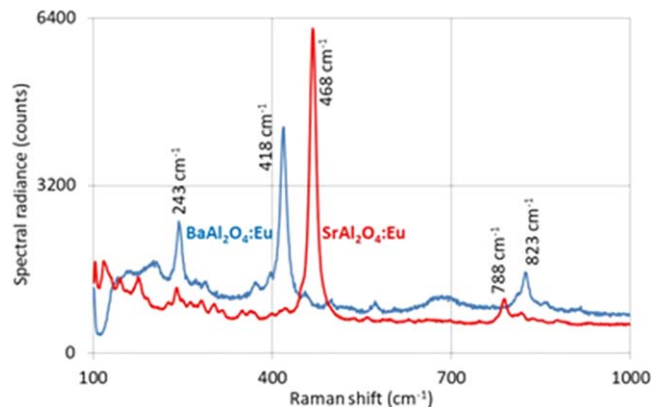

Figure 7. Raman spectra of $BaAl_2O_4$:Eu (BA2) and $SrAl_2O_4$:Eu (SA1) recorded at 25°C.

Discussion

In this section we shall discuss the rather surprising result that $BaAl_2O_4$:Eu reduced in H_2/N_2 at 1350 °C generates only Eu^{3+} luminescence when excited by the green YAG:Nd laser. At this temperature during annealing, even if the dew point of the H_2/N_2 gas would be about 20 °C, the reduction of Eu^{3+} to Eu^{2+} in $BaAl_2O_4$ is expected to be nearly 100% based on thermodynamic considerations. An incomplete reduction of Eu^{3+} in $BaAl_2O_4$/$SrAl_2O_4$ was assumed by Clabau et al.[20] and Rodrigues et al.[21] If a trace of Eu^{3+} would be present in the BA2 sample, Eu^{3+} may directly be excited by the green YAG-Nd laser (18793 cm^{-1}) to the Eu^{3+} $^5D_0$ state at 17262 cm^{-1}. The consequential luminescence of the $^5D_0 \rightarrow {}^7F_J$ transitions is then expected to have the normal thermal behaviour, i.e. decreasing spectral radiance upon increasing the temperature. Since this is not observed in BA2, we assume that the quantity of Eu^{3+} in the sample is so small that it will not lead to detectable Eu^{3+} emission. The conclusion of this reasoning is that the Eu^{3+} luminescence in Figs 2 and 3 has a different origin.

In Fig. 8 the energy levels of Eu^{2+} and Eu^{3+} in $BaAl_2O_4$ that are relevant for the present discussion are presented. For Eu^{2+} the $^8S_{7/2}$ ground state level and the lowest Eu^{2+} 5d level have been depicted, while for the Eu^{3+} ion the ^7F_J levels and the $^5D_0$ level have been indicated. This diagram has been based on the energy diagram for $BaAl_2O_4$:Eu^{2+}, R^{3+} where R is Dy or Nd, reported by Kaur et al.[10]

For a discussion about the Arrhenius plot illustrated in Fig. 3b, the band gap E_g and the position of the Eu^{2+} $^8S_{7/2}$ (ground state) level relative to the valence band (VB), indicated by V in Fig. 8a, needs to be known. The literature is not particularly unanimous about the bandgap (E_g) of $BaAl_2O_4$: it varies between 4.5 and 6.5 eV.[21–24] For Fig. 8a we have adopted E_g=6.5 eV (52430 cm^{-1}) as was done by Kaur et al.[10] Dorenbos[25] described a method for determining the ground state of Eu^{2+} relative to the top of the VB. He argued that it may be positioned at the same level as the Eu^{3+} charge transfer (CT). This latter level is about 4.1 eV above the VB as indicated by Kaur et al.[10] and Wiglusz and Grzyb.[14] When V is set to 4.1 eV, it follows that the lowest Eu^{2+} $4f^65d^1$level would be placed inside the conduction band (CB), which cannot be the case. This conclusion is based on the PL and CL bands of $BaAl_2O_4$:Eu^{2+},[4] which are at 2.5 eV. A way out is to assume that a rather large difference of ≈4000 cm^{-1} (0.5 eV) between the Eu^{3+} CT and the Eu^{2+} $^8S_{7/2}$ levels could be in place, as mentioned by Dorenbos.[25] This uncertainty in the positioning of the ground state of Eu^{2+} (and the other states of Eu^{2+}) relative to the VB of $BaAl_2O_4$:Eu^{2+} renders Fig. 8a slightly speculative. Nevertheless, with this assumption it is plausible that upon laser excitation the lowest 5d level, the $4f^65d^1$level, can be excited according to arrow L. The energy of the laser is not sufficient to reach the $4f^65d^1$level, but due to the thermal population of higher vibronic levels of the $Eu^{2+}$$^8S_{7/2}$ level the lowest 5d level of the Eu^{2+} can be excited, as illustrated in more detail in

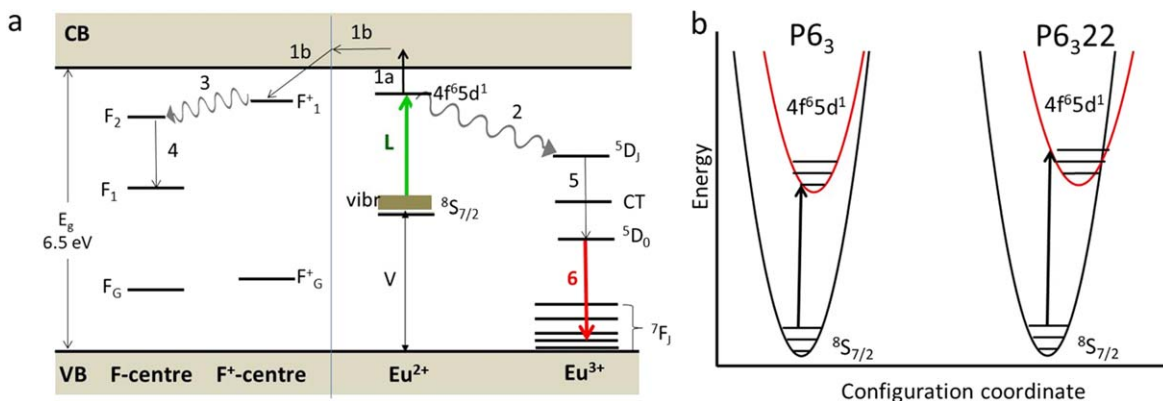**Figure 8.** (a): Energy diagram and bandgap (E_g) of BaAl$_2$O$_4$Eu. CB= conduction band, VB= valence band. Relevant energy levels of Eu^{2+} and Eu^{3+} have been indicated. V is distance of the Eu^{2+8}S$_{7/2}$ level to the top of the VB. L is the laser excitation of the Eu^{2+} ion from the ^{8}S$_{7/2}$ level to the lowest 5d level. The other arrows are explained in the text. (b): Configuration diagrams illustrating the Eu^{2+} excitation by laser from the ^{8}S$_{7/2}$ state to the 4f^{6}5d^{1}state.

Fig. 8b, although the Stokes shift of this Eu^{2+} transition is about 6000 cm^{-1}, as estimated by Poort et al.[26] Excitation of phosphors at energies below the UV PL absorption range has been described in detail by Silver et al. for Y$_2$O$_3$:Eu^{3+} with a He-Ne laser.[27]

The Eu^{2+} 4f^{6}5d^{1}level is assumed to be close to the bottom of the conduction band (CB): in[4] we have determined that the 4f^{6}5d^{1}level is 0.4 eV below the bottom of the CB of BaAl$_2$O$_4$:Eu^{2+}; however, the accuracy of this value is not particularly large due the limited temperature range of the PL measurements. The Eu^{2+} 4f^{6}5d^1 state can also be populated by a two-photon absorption process. Apart from the fact that this process has a low probability, it would also be expected to lead to green Eu^{2+} emission at about 500 nm. Since this emission is not observed, we shall neglect this possibility.

The model presented in Fig. 8a is similar to the electron trapping model that has been used to explain the long decay times in SrAl$_2$O$_4$:Eu^{2+},Dy^{3+} and BaAl$_2$O$_4$:Eu^{2+},Dy^{3+}.[10,18–21,28–30] In this latter model it is generally assumed that Eu^{2+} ions are oxidized to Eu^{3+} by UV excitation and that the released electrons are trapped in defect levels located below the bottom of the CB. The phosphorescence then arises from the recombination of these trapped electrons with the just formed Eu^{3+} ions, generating the characteristic cyan BaAl$_2$O$_4$:Eu^{2+} emission. In our investigations the BaAl$_2$O$_4$ samples did not contain Dy^{3+} and Nd^{3+} ions and the recombination of the trapped electrons with the just formed Eu^{3+} did not occur either. Before considering the fate of the freed electron in the CB via arrow 1a in Fig. 8a, we shall briefly define the F$^+$- and F-centres in BaAl$_2$O$_4$. As described by Lee and Crawford[31], an F-centre in Al$_2$O$_3$, and also in BaAl$_2$O$_4$, may be compared to a He atom, with a doubly charged virtual nucleus, the oxygen vacancy, and two electrons. The quasi He levels will be split according to the local symmetry conditions of the oxygen vacancy. For the present consideration we do not need this complication. An F-centre is thus an oxygen vacancy with two electrons, while an F$^+$-centre is an oxygen vacancy that has trapped one electron. Tentatively we position the excited levels of the F$^+$- and the F-centres just below the bottom of the CB of BaAl$_2$O$_4$, as is done for the F- centre in Al$_2$O$_3$,[31–33] After promotion to the CB (arrow 1a) the electron can drift until it is trapped at an oxygen vacancy, which is doubly charged, or a singly charged F+-centre. Kauer et al.[10] did not indicate that the charge of the oxygen vacancy or F$^+$-centre changes when the electron is absorbed. We have indicated this neutralization process for the F$^+$-centre by arrow 3: the F$^+$-centre becomes an F-centre in the excited state F$_2$. From this F$_2$-state the electron can now relax radiationless to a deep trap as illustrated by arrow 4 between two excited levels of the F-centre. Being locked in this deep trap, it cannot return to the CB by heating the sample. We assume that the concentration of oxygen vacancies and F$^+$-centres in the AlO$_4$ tetrahedra of BaAl$_2$O$_4$:Eu^{2+} is sufficiently large to allow the trapping of the electron indicated by arrow 1b. Annealing of the doped samples in H$_2$/N$_2$ guarantees apparently a sufficient level of oxygen vacancies. This is also the underlying assumption in the long-persistence model for SrAl$_2$O$_4$:Eu^{2+},Dy^{3+} and BaAl$_2$O$_4$:Eu^{2+},Dy^{3+}.[10,18–21,28–30]

The temperature behaviour of the Eu^{3+} emission presented in Figs. 2 and 3 will now be discussed with aid of Fig. 8b. In this latter figure two configuration diagrams are presented, one for the ferroelectric P6$_3$ phase and the other for the paraelectric P6$_3$22 phase. It is assumed that for the P6$_3$22 phase the minimum of the energy curve for the Eu^{2+} 4f^{6}5d^1 state has shifted more than the corresponding minimum for the P6$_3$ phase. This means that more energy is required for exciting 4f^{6}5d^1 state, as can be seen in Fig. 8b. This difference explains the higher activation energy for the Eu^{3+} ^{5}D$_0$ → ^{7}F$_2$ transition indicated in Fig. 3 for the P6$_3$22 phase.

Conclusions

In this paper we have described the changes in the LA and Raman spectra of undoped BaAl$_2$O$_4$ and BaAl$_2$O$_4$:Eu^{2+} that appear at the phase change from the ferroelectric P6$_3$ phase to the paraelectric P6$_3$22 phase. From the analyses of the Raman spectra of BaAl$_2$O$_4$:Eu^{2+} it was concluded that the transition from the P6$_3$ phase to the P6$_3$22 phase takes place at ≈180 °C, which is in good agreement with the results based on totally different methods that were described in the literature. Another interesting finding is that the LA-spectra of BaAl$_2$O$_4$:Eu^{2+} did not contain Eu^{2+} luminescence, but rather Eu^{3+} emission lines/band. This result has been explained by a model that is based on the ionization of the excited 5d state of Eu^{2+} and migration of the freed electron to a deep trap, which is assumed to be an F-centre. The model presented in Fig. 8 also explains qualitatively the two activation energies presented in Fig. 3b and it illustrates the correspondence to the model described.

The work reported herein has provided a new insight to the role and the origin of traps important to the properties of long persistence phosphors as well as those of other non-persistent BaAl$_2$O$_4$:Eu^{2+} phosphors.

References

1. L. Yu, D. den Engelsen, J. Gorobez, G. Fern, T. Ireland, C. Frampton, and J. Silver, *Opt. Mater. Express*, **9**, 2175 (2019).
2. M. Volhard, L. Yu, D. den Engelsen, G. Fern, T. Ireland, and J. Silver, *Opt. Mater. Express*, in press.

3. M. Volhard, D. den Engelsen, G. Fern, T. Ireland, and J. Silver, *Opt. Mater. Express*, **9**, 3895 (2019).
4. D. den Engelsen, G. Fern, T. Ireland, F. Yang, and J. Silver, *Opt. Mater. Express*, in press.
5. S. Kawaguchi, Y. Ishii, E. Tanaka, H. Tsukasaki, Y. Kubota, and S. Mori, *Phys. Rev. B*, **94**, 054117 (2016).
6. S. Y. Huang, R. V. D. Mühll, J. Ravez, and M. Couzi, *Ferroelectrics*, **159**, 127 (1994).
7. S. Y. Huang., R. V. D. Mühll, J. Ravez, J. P. Chaminade, P. Hagenmuller, and M. Couzi, *J. Solid State Chem.*, **109**, 97 (1994).
8. M. Abakumov, O. I. Lebedev, L. Nistor, G. Van Tendeloo, and S. Amelinkx, *Phase Transitions*, **71**, 143 (2000).
9. U. Rodehorst, M. A. Carpenter, S. Marion, and C. M. Henderson, *Mineral. Mag.*, **67**, 989 (2003).
10. J. Kaur, B. Jaykumar, V. Dubey, R. Shrivastava, and N. S. Suryanarayana, *Res. Chem. Intermed.*, **41**, 2317 (2015).
11. W. Hörkner and H. K. Müller-Buschbaum, *Z. Anorg. Allg. Chem.*, **451**, 40 (1979).
12. A.-R. Schulze and H. Müller-Buschbaum,, *Z. Anorg. Allg. Chem.*, **475**, 205 (1981).
13. R. Chatterjee, S. Saha, D. Sen, K. Panigraphi, U. K. Ghorai, G. C. Das, and K. K. Chattopadyay, *ACS Omega*, **3**, 788 (2018).
14. R. J. Wiglusz and T. Grzyb, *Opt. Mater.*, **36**, 539 (2013).
15. T. Jansen, D. Böhnisch, and T. Jüstel, *ECS J. Solid State Sci. Technol.*, **5**, R91 (2016).
16. O. B. Shchekin, P. J. Schmidt, F. Him, N. Lawrence, K. J. Vampola, H. Bechtel, D. R. Chamberlin, R. Mueller-Mach, and G. O. Mueller, *Phys. Status Solidi RRL*, **10**, 310 (2016).
17. B. Lazic, V. Kahlenberg, R. Kaindl, and A. Kremenovic, *Solid State Sci.*, **11**, 77 (2009).
18. G. Dong, X. Xiao, L. Zhang, Z. Ma, X. Bao, M. Peng, Q. Zhang, and J. Qiu, *J. Mater. Chem.*, **21**, 2194 (2011).
19. H. Terraschke, M. Suta, M. Adlung, S. Mammadova, N. Musayeva, R. Jabbarov, M. Nazarov, and C. Wickleder, *J. Spectroscopy*, **2015**, 541958 (2015).
20. F. Clabau, X. Rocquefelte, S. Jobic, P. Deniard, M.-H. Whangbo, A. Garcia, and T. L. Mercier, *Chem. Mater.*, **17**, 3904 (2005).
21. L. C. V. Rodrigues, J. Hölsä, J. M. Carvalho, C. C. S. Pedroso, M. Lastusaari, M. C. F. C. Felinto, S. Watanabe, and H. F. Brito, *Physica B*, **439**, 67 (2014).
22. L. Zhang, L. Wang, and Y. Zhu, *Adv. Funct. Mater.*, **17**, 3781 (2007).
23. H. Wako, F. B. Dejene, and H. C. Swart, *J. Rare Earths*, **32**, 806 (2014).
24. L. C. V. Rodrigues, R. Stefani, H. F. Brito, M. C. F. C. Felinto, J. Hölsä, M. Lastusaari, T. Laamanen, and M. Malkamaki, *J. Solid State Chem.*, **183**, 2365 (2010).
25. P. Dorenbos, *J. Phys. Condens. Matter*, **15**, 8417 (2003).
26. S. H. M. Poort, W. P. Blokpoel, and G. Blasse, *Chem. Mater.*, **7**, 1547 (1995).
27. J. Silver, M. I. Martinez-Rubio, T. G. Ireland, G. R. Fern, and R. Withnall, *J. Chem Phys. B*, **105**, 9107 (2001).
28. E. Nakazawa, Y. Murazaki, and S. Saito, *J. Appl. Phys.*, **100**, 113113 (2006).
29. P. Dorenbos, *J. Electrochem. Soc.*, **152**, H107 (2005).
30. H. F. Brito, M. C. F. C. Felinto, J. Hölsä, T. Laamanen, M. Lastusaari, M. Malkamäki, P. Novák, L. C. V. Rodrigues, and R. Stefani, *Opt. Mater. Express*, **2**, 420 (2012).
31. K. H. Lee and J. H. Crawford Jr, *Phys. Rev. B*, **19**, 3217 (1979).
32. B. G. Draeger and G. P. Summers, *Phys. Rev. B*, **19**, 1172 (1979).
33. P. Jonnard, C. Bonnelle, G. Blaise, G. Rémond, and C. Roques-Carmes, *J. Appl. Phys.*, **88**, 6413 (2000).